Chemical Engineering Journal Advances 25 (2026) 101053

Contents lists available at ScienceDirect

Chemical Engineering Journal Advances

journal homepage: www.sciencedirect.com/journal/chemical-engineering-journal-advances

Representative secondary PET micro and nanoplastics via ethylene glycol fragmentation (EGF): Physicochemical and immuno-toxicological properties

Mohammed Monsoor Shaik [a], Diletta Ami [a], Alessio Romerio [a], Calogero Gagliano [a], Charys Palmer [b], Zaineh Aladailleh [b], Elijah Mitchell [b], Janet Lopez Chavez [b], Asma Zain [b], Stefano Farris [c], Mattia Gaboardi [d,e], Antonino Natalello [a], Grisha Pirianov [b], Francesco Peri [a,*]

[a] Department of Biotechnology & Biosciences, University of Milano-Bicocca, Italy
[b] Faculty of Science and Engineering, School of Life Sciences, Anglia Ruskin University, Cambridge, United Kingdom
[c] Department of Food, Nutrition and Environmental Sciences, University of Milan, Italy
[d] Physics Department, University of Rome Tor Vergata, via della Ricerca Scientifica 1, Roma, Lazio 00133, Italy
[e] INFN – Rome Tor Vergata, via della Ricerca Scientifica 1, Roma, Lazio 00133, Italy

ARTICLE INFO

Keywords:
Polyethylene terephthalate (PET)
Micro and nanoplastics (MNPs)
Glycolysis
Physicochemical characterization
BHET oligomers
macrophages
immunotoxicology

ABSTRACT

Polyethylene terephthalate (PET) micro and nanoplastics (MNPs) are widely dispersed pollutants with significant environmental and health implications. Current preparation methods of representative secondary PET MNPs are limited. In this study, we developed a scalable, standardized ethylene glycol fragmentation (EGF)-based method to generate PET MNPs from three distinct plastic sources (commercial pellets, bottle-grade, and film-grade). PET samples were depolymerized using ethylene glycol and sodium carbonate under controlled thermal conditions. Two fractions (Ea and Eb) were collected and analyzed, fraction Ea consisted of covalently fragmented BHET-oligomer-based nanoplastics (~200–375 nm), while fraction Eb comprised non-covalent BHET-based larger microplastic aggregates (~1.2–1.9 μm). EGF method turned out to be more efficient than published trifluoroacetic acid (TFA) method giving mainly BHET-oligomer-based nanoplastics with higher yields and improved MNPs size control. MNPs generated by EGF showed a size range between 200 and 375 nm with good colloidal stability. In vitro assays showed that both type (covalent and non-covalent) of PET nanoplastics reduced THP-1 macrophage viability in a dose-dependent manner which was associated with IL-1β release, and triggered an M1-polarizing cytokine profile, thus indicating potential toxicity and proinflammatory activity. Our EGF-based synthesis platform enables controlled production of PET MNPs with source-dependent characteristics and biologically relevant behavior. These standardized MNPs and the THP-1 macrophages biosensor model provide useful tools for environmental toxicology research.

1. Introduction

The widespread production and use of plastics has led to their ubiquitous presence in plastic waste streams [1]. Micro-nanoplastics (MNPs) originating from the degradation of macroplastics persist in diverse environments, and further fragment into nanoplastics (NPs) which can interact with biological systems. These interactions have shown to induce oxidative stress, inflammation, and cellular damage in different biotic models [2–5]. As a thermoplastic polymer widely used in packaging, textiles, and consumer goods, polyethylene terephthalate

Abbreviations: AFM, atomic force microscopy; ATR-FTIR, attenuated total reflection Fourier transform infrared; BHET, bis(2-hydroxyethyl) terephthalate; Credit, contributor roles taxonomy; DLS, dynamic light scattering; EGF, ethylene glycol fragmentation; ELISA, enzyme-linked immunosorbent assay; LDH, lactate dehydrogenase; MNPs, Micro- and Nanoplastics; MTT, 3-(4,5-dimethylthiazol-2-yl)-2,5-diphenyltetrazolium bromide; PDI, Polydispersity Index; PET, Polyethylene terephthalate; SDS, Sodium Dodecyl Sulfate; TEM, Transmission Electron Microscopy; TPA, Terephthalic Acid; TFA, Trifluoroacetic Acid.

* Corresponding author.
E-mail address: francesco.peri@unimib.it (F. Peri).

https://doi.org/10.1016/j.ceja.2026.101053

Available online 22 January 2026

(PET) accounts for approximately 12 % of global plastic production. Its annual output exceeds 55 million tons [6,7]. Despite its recyclability, its widespread use, improper disposal and environmental degradation contribute significantly to microplastic pollution [8,9]. However, the biological impact of PET MNPs remains poorly understood, in part due to a lack of standardized, representative materials for toxicological studies. Plastics are susceptible to degradation via abiotic mechanisms due to different factors such as thermal and photodegradation and mechanical abrasion [10–12]. Fig. 1 provides a schematic representation of different possible PET chemical fragmentation MNPs generated through ester bond cleavage. PET from commercial, bottle-grade, or film-grade sources exhibits considerable differences due to variations in additives, crystallinity, and intrinsic viscosity [13,14].

Different recycling methods for PET have been reported, where the polymer is fully fragmented through acid hydrolysis or glycolysis until reusable monomers are obtained [15–17]. Metal-Organic Framework-based catalytic routes for PET chemical recycling have also been explored with the aim of repurposing PET monomers for energy storage applications [18,19]. Among these, the trifluoroacetic acid (TFA)-based hydrolysis protocol has also been applied to the generation of PET NPs [20]. This acid-based hydrolysis partially depolymerizes PET, disrupting crystalline regions and leading to the formation of terephthalic acid (TPA)- or mono(2-hydroxyethyl) terephthalate (MHET)-based oligomers. While many researchers have employed the same TFA protocol for PET NP production, its practical limitations, including low yields and slow kinetics, remain significant challenges [21,22]. Despite this published method to obtain PET NPs by acid hydrolysis, currently, no standard PET MNPS are commercially available for biological studies.

Here we present a new protocol to obtain PET NPs based on ethylene glycol fragmentation (EGF) in the presence of sodium carbonate [23]. We prepared PET NPs from three different sources: PET Commercial (PC), PET bottle-grade (PB), and PET film-grade (PF). Comprehensive physicochemical and biological characterization were conducted to assess the properties and potential impacts of PET NPs. Comparisons with TFA-based hydrolysis were made to highlight the advantages of the EGF method in terms of efficiency, scalability, and environmental relevance. We utilized THP-1 macrophage polarization model as a biosensor for the assessment of proinflammatory properties of generated PET NPs. The findings contribute to advancing standardized NPs reference materials for environmental and toxicological research.

2. Materials and methods

2.1. Materials

Three types of PET were used as starting materials: commercial PET (Goodfellow, particle size ~300 μm, crystallinity <50 %), bottle-grade PET (sourced from food-grade supplier, unused, crystallinity 40–45 %), and film-grade PET (obtained from food packaging films, crystallinity ~30 %). Bis(2-hydroxyethyl) terephthalate (BHET) and terephthalic acid (TPA) were used as MNP reference standards (Sigma-Aldrich, purity ≥94 %). Ethylene glycol (EG, 99.5 %) and sodium carbonate (Na_2CO_3, 99.9 %) were used in the EGF reactions. Milli-Q water was used throughout the study to minimize contamination.

2.2. Preparation of PET MNPs

To perform the EGF reaction, 1 g of PET (PC/PB/PF) was added to 2.2 mL of ethylene glycol along with 30 mg of sodium carbonate in a round-bottom flask. The mixture was heated to 185 °C under constant stirring (600 – 800 rpm) to ensure homogeneous mixing. The reaction was allowed to proceed for 4 h before being terminated by adding 10 mL of Milli-Q water dropwise under stirring. The resulted precipitate was then filtered using glass microfiber filters (Whatman® GF, pore size <1.0 μm) and air-dried at 55 °C for 24 h, the solid residue was labelled as fraction Ea. The residual clear filtrate was kept at 4 °C overnight for precipitation. The mixture was filtered again using the same glass microfiber filters and the collected residue was labelled as fraction Eb.

2.3. Physicochemical characterization

2.3.1. Dynamic light scattering (DLS) and zeta potential

Particle size distribution and zeta potential were measured using a NanoBrook 90Plus Zeta instrument. Samples were dispersed in Milli-Q water, and measurements were conducted at 25 °C. Three replicates were recorded for each sample to ensure reproducibility.

2.3.2. Transmission electron microscopy (TEM)

TEM was performed using a Hitachi HT7800 instrument operating at 100 kV equipped with QEDIRA B60T camera (EMSIS Münster, Germany). All the PET MNP samples (PC; PB; PF) of both Fraction Ea and Fraction Eb were diluted in Milli-Q water and applied onto glow-discharged, carbon-coated copper grids. Each sample was adsorbed for 2 min, excess liquid was blotted, and the grids were stained with 1 % (w/v) phosphotungstic acid as a negative stain. After a 30-second incubation, grids were blotted and allowed to air dry at room temperature. Representative images were acquired at 20,000 × magnification.

2.3.3. Attenuated total reflection-Fourier transform infrared (ATR-FTIR) spectroscopy

For ATR-FTIR analyses, samples were placed on the diamond crystal of a single reflection ATR accessory (Quest, Specac, USA) and forced into

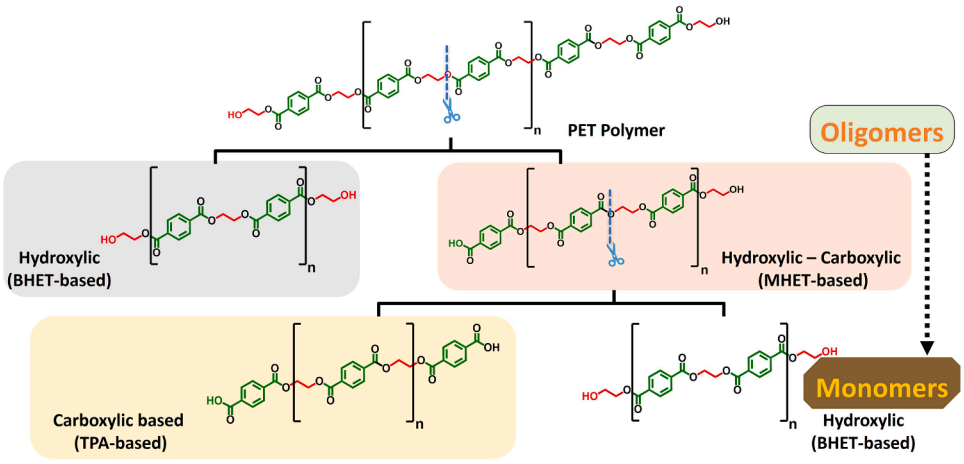

Fig. 1. Schematic representation of different possible PET MNPs generated by random ester bond cleavage.

close contact with the crystal using the clamp arm assembly of the device [24,25]. ATR-FTIR spectra were recorded at room temperature using a Varian 670-IR spectrometer (Varian Australia Pty Ltd., Mulgrave, VIC, Australia) equipped with a nitrogen-cooled mercury cadmium telluride (MCT) detector. Measurement parameters were: 2 cm^{-1} spectral resolution, 25 kHz scan speed, 512 coadded scans, and triangular apodization. The figures display the average FTIR spectra, calculated from three independent analyses per sample. Spectra were normalized at the peak of maximum absorption in the displayed spectral range.

2.3.4. Atomic force microscopy (AFM)

AFM measurements were performed on the Ea fractions using the Horiba OmegaScope optical platform equipped with gold tips (μMASCH) with 150 μm cantilever Samples diluted in H_2O were deposited onto a flat Si chip and let dry for a few minutes without any additional treatment. A 100 × objective was used for accurate localization of the region of interest, and AFM scans were conducted in tapping mode at room temperature. Standard AFM parameters such as scan rate and resolution were optimized to obtain high-quality surface topography data while minimizing tip–sample interaction. Raw AFM images were processed and analyzed using Gwyddion software, which enables data flattening, artifact filtering, and the extraction of quantitative surface parameters [26].

2.4. Biological assays

2.4.1. Cells maintenance and treatment

THP-1 cells were obtained from the European Collection of Animal Cell Cultures (Salisbury, Wiltshire, U.K.) and cultured in RPMI (+10 % heat inactivated foetal bovine serum (HIFBS), +1 % Glutamine, +1 % penicillin/streptomycin). Cells were split 3 times weekly and maintained at a density of ~0.5×10^6 cells/ml. For differentiation of THP-1 cells, 25 nM of PMA (Phorbol 12-myristate 13-acetate) was added to plated cells for 3 days before washing three times with fresh medium. Cells were then left to rest overnight before the THP-1 macrophages were exposed to PET (0–5mg/ml) for 24 h.

2.4.2. MTT assay

MTT assay was performed to evaluate the effect of MNP samples on THP-1 derived macrophage viability. Cells were treated with different concentrations of PET MNP (0–5mg/ml). MTT was dissolved in RPMI 1640 medium (5mg/ml). Subsequently, 25 μl of the MTT solution was added to each well of a 96-well plate, containing 50,000 cells per well. The cells were then incubated at 37 °C with 5 % CO_2 for 2 h. A blank control solution was prepared by using complete medium without cells. Finally, cells were solubilised with 10 % SDS and incubated overnight at 37 °C. 100 ml medium from each well was spun down (5000 g) and the supernatant was transfer in new 96 well plate. Plates were read at absorbance wavelength of 620 nm.

2.4.3. LDH assay

To assess the effect of PET MNP samples on THP-1 macrophage viability associated with pyroptosis, LDH assay was used. THP-1 macrophages were seeded on 96 well plates (0.5×10^6/ml). Cells were differentiated with PMA (25 nM) for 3 days. PMA was washed out and THP-1 macrophages were left for 24 h in fresh medium before to exposed to PET MNP (0–5mg/ml) for further 24 h. 10 μl medium from each sample/well was analysed for LDH release following manufacturer's instructions (Abcam, UK). Finally, plates were read at 450/620 nm.

2.4.4. Inflammation antibody array

THP-1 macrophages were treated with PET MNP samples. Culture medium was collected after 18 h of incubation and analysed on a human inflammation array (Ray-Biotech, USA) containing 40 proinflammatory proteins) to assess relative levels of cytokine expression by samples. Results are expressed as fold-increase relative to control samples.

2.4.5. ELISA

Human IL-1β production was measured in cell culture medium using ELISA kits (R&D Systems, USA and Ray-Biotech, USA) following the manufacturer's instructions. At the final stage, absorbance was measured at 450 nm using the Sunrise (Tecan Group LTD., Switzerland) microplate reader. Protein concentration was calculated using GraphPad Prism version 7.01.

3. Results and discussion

3.1. Preparation of PET MNPs

The ethylene glycol fragmentation (EGF) method described here for preparing the PET-derived MNPs employed ethylene glycol under controlled heating conditions in the presence of sodium carbonate. Two distinct fractions were collected by filtration and labelled as fraction Ea and fraction Eb. Fraction Ea accounted for 27–33 % of the total mass, while fraction Eb comprised 67–73 %. In comparison, the previously reported TFA hydrolysis method showed significantly lower yields (approximately 5 %) and primarily produced TPA-based oligomers. Fraction Ea turned out to be BHET-based PET fragments representing well secondary PET MNP generated by chemical or physical or mechanical fragmentation. This is in accordance with the fact that EGF method is based on a transesterification reaction, and ethylene glycol cleaves PET's ester bonds yielding BHET-based oligomers [23]. Fraction Eb, is constituted by PET monomers aggregated through non-covalent interactions in large particles (thousand nm size) representing the microplastic fraction of MNPs. This partitioning reflects the efficiency of EGF in producing distinct oligomeric and monomeric fractions. It must be noted that the separation of fractions Ea and Eb by filtration is not strictly due to size cutoff of the filter, but is driven by differences in the solubility and aggregation behavior of the depolymerization products in the aqueous medium. Fraction Ea precipitates first because it consists of covalently stable, higher molecular weight PET residues that are essentially insoluble in the polar aqueous environment (water/ethylene glycol mixture). Upon the addition of water, these hydrophobic, high-*Mw species*immediately aggregate into micron-scale particles (MNPs), causing the observed rapid precipitation. The low molecular weight species (such as BHET monomers and possibly small oligomers) remain soluble in hot polar environment and pass through the filter during the first filtration. As the temperature of solution cools, the low-*M.species*reach the supersaturation and gradually crystallize or aggregate into large particles which can filtered as fraction Eb [27,28]. The filtration-based separation effectively exploits the different stability and aggregation states of the two fractions in water thereby generating PET NPs (fraction Ea) as well as larger PET microplastic derived from monomers aggregation (fraction Eb).

The EGF mechanism is different from acid hydrolysis (TFA method), which preferentially generates carboxylic acid-terminated oligomers (TPA-based) due to ester bond acid hydrolysis [16,20]. The transesterification route of EGF offers superior control over the depolymerization process, resulting in more uniform oligomer distributions and higher yields [17,29]. Such controlled glycolytic depolymerization aligns with literature demonstrating similar efficacy and selectivity in PET breakdown using glycol solvents. In contrast, the TFA method relies on hydrolysis of PET in concentrated trifluoroacetic acid at lower temperatures (50 °C), typically inducing rapid yet heterogeneous depolymerization. This method is known to yield TPA-rich oligomers exposing carboxylic acid functionalities. Our FTIR analysis confirms that with the TFA hydrolysis protocol TPA fragments are formed and show chemical structures different from the BHET-based fragments obtained via EGF method [30,31].

Our replication of this method, conducted both with and without

SDS, highlighted particle sizes in the same order of magnitude in the two conditions (Fig. S1 and Fig. S2). In contrast with the existing methods, EGF protocol allows to obtain SDS-free standard PET MNPs that are homogenously dispersed in aqueous media [20]. This aligns with recent literature advocating for the production of environmentally relevant microplastics free from surfactants that may alter natural interactions [32,33]. The possibility of using MNPs not contaminated by SDS is relevant because SDS is toxic for cells and animals and therefore impacts in the outcome of biological evaluation of MNPs [32,34]. In general, SDS-free MNPs better represent environmental MNP and are better standards to study their biological properties through cell or animal experiments [33,35].

The environmental and interactional implications of these chemically distinct PET oligomers are substantial. BHET-based oligomers terminate by neutral hydroxyl groups, so that the corresponding MNPs present neutral group on their surface. On the contrary, MNP obtained by TFA-mediated acid hydrolysis present TPA oligomers with carboxylate ends that are anionic at neutral pH. Such differences in terminal functional groups significantly influence environmental fate, biological uptake, and potential toxicological responses [36,37]. Both fractions were, therefore, subjected to detailed physical characterization (DLS, Zeta, and FTIR) to elucidate their oligomeric nature and potential environmental relevance.

3.2. Physicochemical characterization of PET MNPs

DLS analysis revealed distinct differences in the particle hydrodynamic diameter among the PET MNP samples. The effective diameters of the fractions Ea from different PET sources (PC, PB, PF) were significantly smaller compared to Eb fractions. Specifically, fractions from commercial PET (PC-Ea) exhibited an effective diameter of 345 nm with a polydispersity index (PDI) of 0.35, while PET bottle fractions PB-Ea had a slightly larger diameter of 374 nm and identical PDI (0.35). Finally, the film-derived PF-Ea showed the smallest diameter of 275 nm with a notably lower PDI of 0.26, suggesting greater homogeneity in particle size distribution.

Despite the increase in size, the PDI values remained relatively consistent across fraction Eb samples, ranging from 0.35 to 0.38, indicating moderate size distribution uniformity. ζ-potential measurements showed relatively consistent among fraction Ea samples from different PET sources, ranging from −34 mV to −36 mV (Table 1). This suggests good colloidal stability, resistance to particle aggregation and better environmental dispersion [37]. Fractions Eb demonstrated slightly less negative zeta potentials, with a notably higher value of −27 mV for PF-Eb indicating potentially decreased colloidal stability, suggesting potential agglomeration tendencies due to less negative zeta potentials [36]. This finding is critical, as particle size and colloidal stability significantly influence the environmental fate, bioavailability, and toxicity profiles of MNPs

The TEM analysis revealed further details of particle morphology and dispersion of PET MNPs prepared by EGF method (Fig. 2). Fraction Ea samples from PC (Fig. 2A), PB (Fig. 2B), and PF (Fig. 2C) appeared as dispersed, low-contrast nanostructures with irregular shapes lacking directional structure. The estimated diameters range from ~200 to 400 nm, consistent with DLS results. The irregular morphology of fraction Ea reflects fragmentation into BHET-based oligomers that remained consistent with limited crystalline order as in the FTIR spectra. Fraction Eb samples (Fig. 2D-F), on the other hand, appeared as denser, higher-contrast rod-shaped aggregates with diffuse edges and size around ~1 μm. The morphology and density profile of Eb particles suggest loose supramolecular association, likely driven by BHET stacking and hydrogen bonding.

Table 1
Effective diameter, PDI and ζ- potential of the all the residues of different PET sample types.

Sample ID	Eff. Diameter (nm)	Std. Dev.	PDI	Zeta Potential (mV)
PC-Ea	345	4.21	0.35	−34
PB-Ea	374	10.53	0.35	−34
PF-Ea	275	8.59	0.26	−36
PC-Eb	1350	13.17	0.38	−33
PB-Eb	1497	19.81	0.35	−32
PF-Eb	1880	20.03	0.37	−27

Additionally, we observed that the filtrates corresponding to the fractions Eb, when stored at 4 °C for 24 h, resulted in a visible precipitation. This behavior suggests that low-molecular-weight PET monomers, particularly BHET, may undergo temperature-dependent aggregation or crystallization. Such precipitation tendencies are likely a result of supramolecular interactions and the inherent thermodynamic instability of BHET in aqueous media [38]. These phenomena may explain the larger hydrodynamic diameters observed for fraction Eb. In contrast, the oligomer-rich fraction Ea remained well-dispersed and colloidally stable. These structural characteristics may influence environmental behavior of plastic particles, where fraction Ea might remain suspended and provide enhanced bioavailability, whereas fraction Eb may sediment and accumulate locally [39].

3.3. ATR-FTIR spectroscopy characterization of PET MNPs

To facilitate the interpretation of the PET sample analysis, FTIR investigation was initially conducted on control BHET and TPA standard nanoparticle samples (Fig. 3). The resulting spectra (Fig. 3A) were divided into three distinct regions, that is ~ 4000–2500, 1800–1550, 1500–750 cm^{-1} hereafter named for simplicity hydroxyl, carbonyl and fingerprint regions respectively, to better visualize the differences between the two compounds (Fig. 3B-D). FTIR spectroscopy revealed that the chemical structures of PET were preserved after EGF, albeit with critical differences in crystallinity and amorphous content. Specifically, bottle-derived PB-Ea MNPs retained significant crystalline character, consistent with AFM observations of sharp-edged, irregular particles indicative of crystalline fragmentation behavior. As shown in Fig. 3B, monomeric BHET exhibits a prominent hydroxyl stretching band around 3442 cm^{-1} (Fig. 3B) and two sharp, well-resolved bands in the carbonyl stretching region at approximately 1713 cm^{-1} and 1687 cm^{-1} (Fig. 3C) [29,30]. In contrast, the TPA spectrum displays a broad and intense carbonyl absorption band near 1673 cm^{-1}, with a shoulder around 1610 cm^{-1} and a well resolved peak at ~1575 cm^{-1}, both mainly ascribable to benzene ring vibrations (Fig. 3C), alongside fingerprint region bands near 926 cm^{-1}, primarily due to CH vibrations, and around 780 cm^{-1}, mainly from C—COOH vibrations (Fig. 3D) [31]. Such correlation between crystalline content and sharper-edged morphology has been previously documented in polymer fragmentation studies [40].

We then measured the IR absorption of the commercial, bottle, and film PET MNP residues, which were collected after the first filtration step (Fig. 4). In Fig. 4A the spectra of the three samples are displayed across the entire measured mid-IR spectral range. As discussed above for the standards, the spectra were divided into three spectral regions (Fig. 4B-D). In the 4000–2500 cm^{-1} range (Fig. 4B), fraction Ea from PC, PB, and PF displayed a broad, asymmetric hydroxyl stretching band, characterized by a main peak at approximately 3390 cm^{-1} and additional components at 3440 and 3535 cm^{-1}. The co-occurrence of these three absorption features suggests the presence of BHET-based oligomers [29,30,41].

In the carbonyl region (Fig. 4C), all three samples show a main peak at approximately 1714 cm^{-1}; additionally, a peak at 1700 cm^{-1} is clearly visible in PB-Ea and PF-Ea whereas it appears as a shoulder in PC-Ea [42]. The peaks of the carbonyl stretching mode in the 1800–1550 cm^{-1} region suggest the presence of BHET oligomers, complementing the presence of the hydroxyl stretching bands in the 4000–2500 cm^{-1} region. Furthermore, analysis of the 1500–750 cm^{-1} fingerprint region (Fig. 4D) provided two distinct insights. Firstly, we found no evidence of TPA in any of the three samples (see TPA standard spectrum in Fig. 3D).

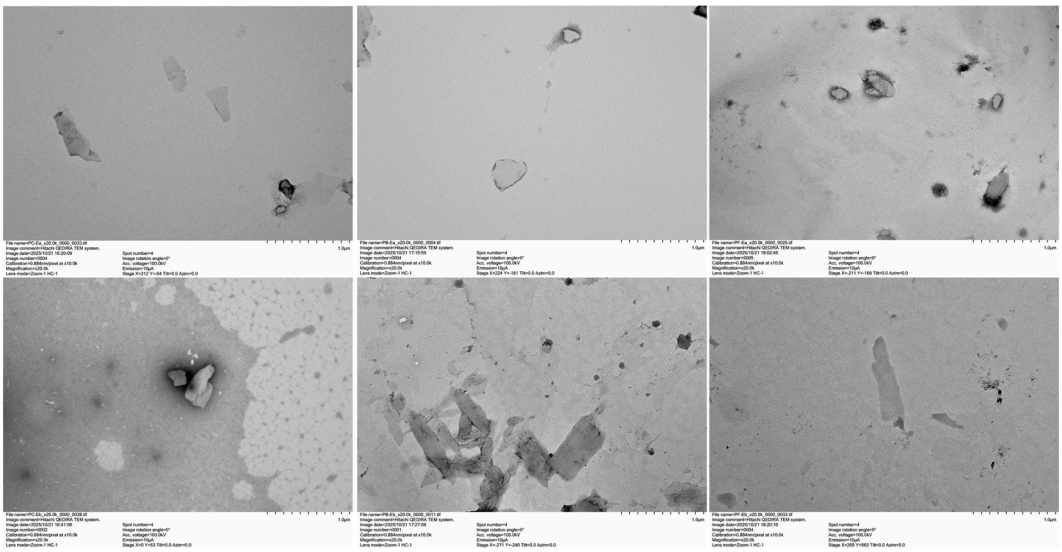

Fig. 2. TEM images of PC-Ea (A), PB-Ea (B), PF-Ea (C), PC-Eb (D), PB-Eb (E), and PF-Eb (F), MNPs obtained via ethylene glycol fragmentation. All images were acquired at 20,000x magnification with phosphotungstic acid negative staining.

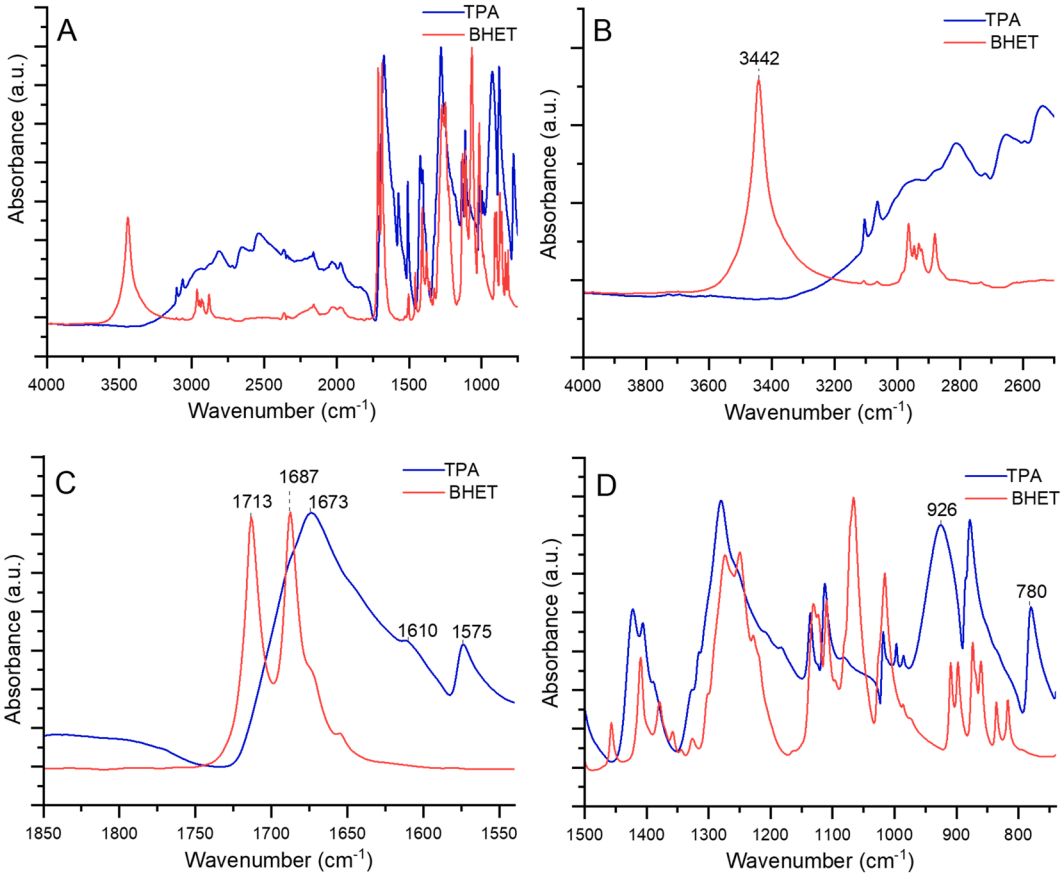

Fig. 3. Mean FTIR absorption spectra of BHET and TPA standard are shown in the full measured range (A), hydroxyl (B), carbonyl (C), and fingerprint (D) regions. In each spectral range, spectra have been normalized to maximum intensity. The relevant peaks are indicated.

Moreover, the simultaneous occurrence of three well-resolved peaks at ~1470 cm^{-1} (CH_2 bending) ~1342 cm^{-1} (CH_2 wagging) and ~972 cm^{-1} (O—CH_2 and C(=*O*)-O stretching) was observed across all samples. These peaks are typically assigned to vibrations of the *trans* conformation of the ethylene glycol moiety, suggesting a high level of crystallinity [30,43].

Next, we analyzed the mid-IR absorption of fractions Eb (Fig. 5), collected after the second filtration. In the 4000–2500 cm^{-1} range (Fig. 5B), FTIR spectra of fractions Eb from PC, PB, and PF primarily showed a band at 3440 cm^{-1}, characteristic of monomeric BHET (see also Fig. 3B). A distinct, though low-intensity, band at 3535 cm^{-1} was observed only in the PC-Eb spectrum, suggesting the additional presence

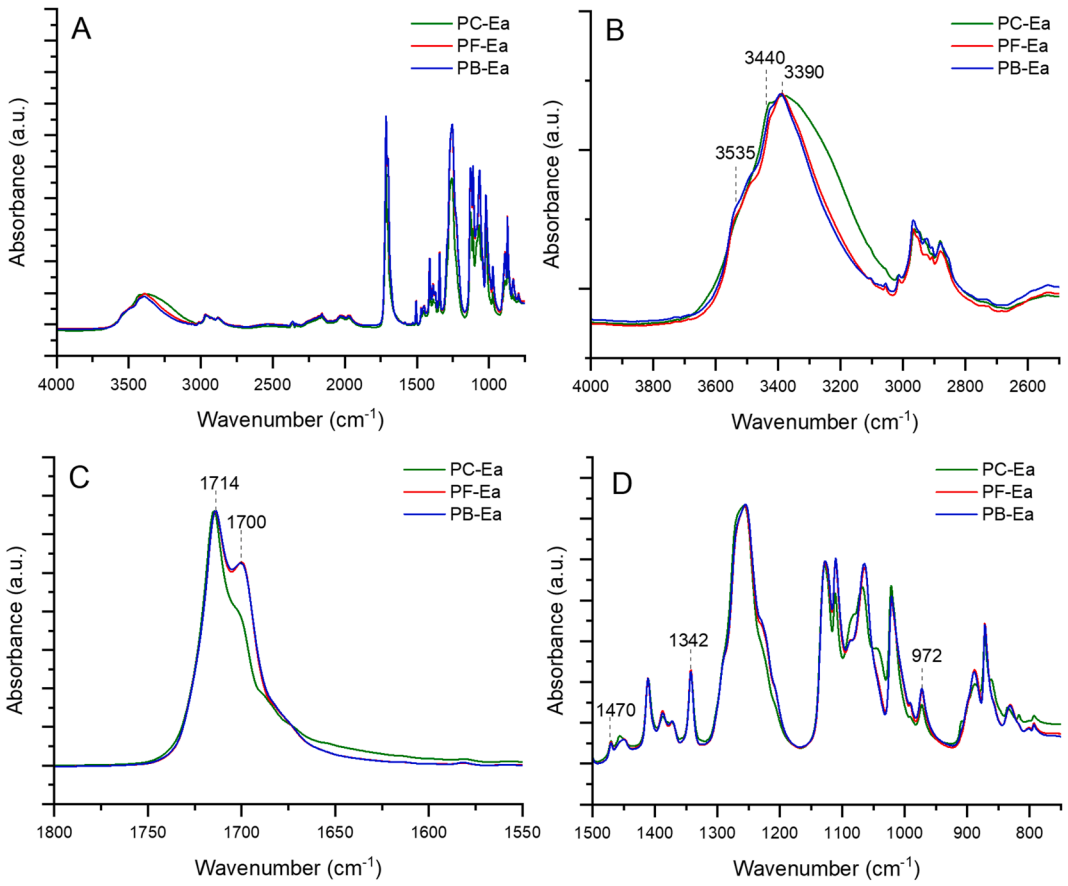

Fig. 4. Mean FTIR absorption spectra of PC, PB, PF collected after the first filtration step (fraction Ea) are shown in the full measured range (A), hydroxyl (B), carbonyl (C), and fingerprint (D) regions. In each spectral range, spectra have been normalized to maximum intensity. The relevant peaks are indicated.

of oligomeric forms. The carbonyl stretching region (Fig. 5C) of the fraction Eb spectra displayed two sharp peaks at approximately 1714 cm^{-1} and 1687 cm^{-1}, consistent with monomeric BHET (Fig. 3C). Furthermore, in the fingerprint region (Fig. 5D) the TPA marker bands were not detected in all three samples (see also Fig. 3D). In contrast to the fraction Ea samples, the ~1470 cm^{-1}, ~1342 cm^{-1}, and ~972 cm^{-1} bands were not detected, suggesting a decrease in crystallinity. Furthermore, the fraction Eb samples exhibited a split band with peaks at approximately 909 cm^{-1} (chain CH_2 rocking) and 898 cm^{-1} (chain CH_2 rocking), a feature absent in fraction Ea. The co-presence of these two peaks, assigned to *trans* and *cis* CH_2 vibrations respectively, indicates more amorphous materials [30,43].

We also analyzed the IR absorption spectra of commercial PET Commercial (PC-Ta), PET bottle (PB-Ta), and PET film (PF-Ta) samples after acid hydrolysis with TFA. We compared these spectra with those of their respective controls (see Fig. S3, Fig. S4 and Fig. S5) and observed the presence of carboxylate end groups, not present in the EGF samples.

Upon examining the entire analyzed range for PC-Ta (Fig. S3 A-D), we did not detect any marker bands indicative of BHET monomers as expected. Instead, in the carbonyl region, we observed two bands that could be attributed to TPA: a broad absorption at approximately 1681 cm^{-1}, which could encompass the spectral components found in the TPA spectrum at approximately 1673 cm^{-1} and 1611 cm^{-1}, as well as a component at approximately 1577 cm^{-1} (Fig. S4 C and Fig. 3C). Furthermore, we also detected an absorption at approximately 780 cm^{-1}, although with low intensity (Fig. S3 D). Very similar spectral features were observed for PF-TB and PB-TB (Fig. S4 and Fig. S5), suggesting the presence of TPA traces but not BHET monomers in these samples as well.

3.4. AFM analysis

Atomic Force Microscopy (AFM) provided insights into the morphology, surface texture, and particle dimensions of the PET-derived MNPs synthesized via EGF (Fraction Ea of PC, PB, PF). The analysis revealed distinct morphological features (Fig. 6), clearly associated with their original PET starting material forms prior to depolymerization. The PC-Ea samples (Fig. 6A) exhibited predominantly circular and spheroidal morphologies, with smooth, regular contours consisting of particles derived from pelletized starting materials. The homogenous, smooth-edged shape observed in these MNPs could be attributed to the uniform initial pelletized material structure and controlled depolymerization kinetics. Such shapes are commonly reported for nanoparticles originating from industrial-grade, uniformly molded polymer pellets due to their consistent density and crystallinity profiles [44]. Conversely, PB-Ea samples (Fig. 6B) displayed irregular and jagged shapes, characterized by pronounced sharp edges and a broader size distribution. This structural irregularity and edge prominence are indicative of crystalline PET structures commonly found in commercial bottles. The presence of sharp edges in MNPs derived from bottle-grade PET aligns well with previously documented crystallinity-dependent fracture patterns during mechanical and chemical processing of crystalline polymers [40]. Film-derived PF-Ea samples (Fig. 6C) revealed highly fragmented and finely dispersed powder-like morphologies. The rapid depolymerization of PET films, accelerated by their significantly greater exposed surface area, resulted in the generation of amorphous particles characterized by irregular, less defined edges compared to the bottle-derived samples. The colloid-like morphology is consistent with literature reports documenting rapid surface degradation and fragmentation behavior of polymer films under chemical treatments, driven

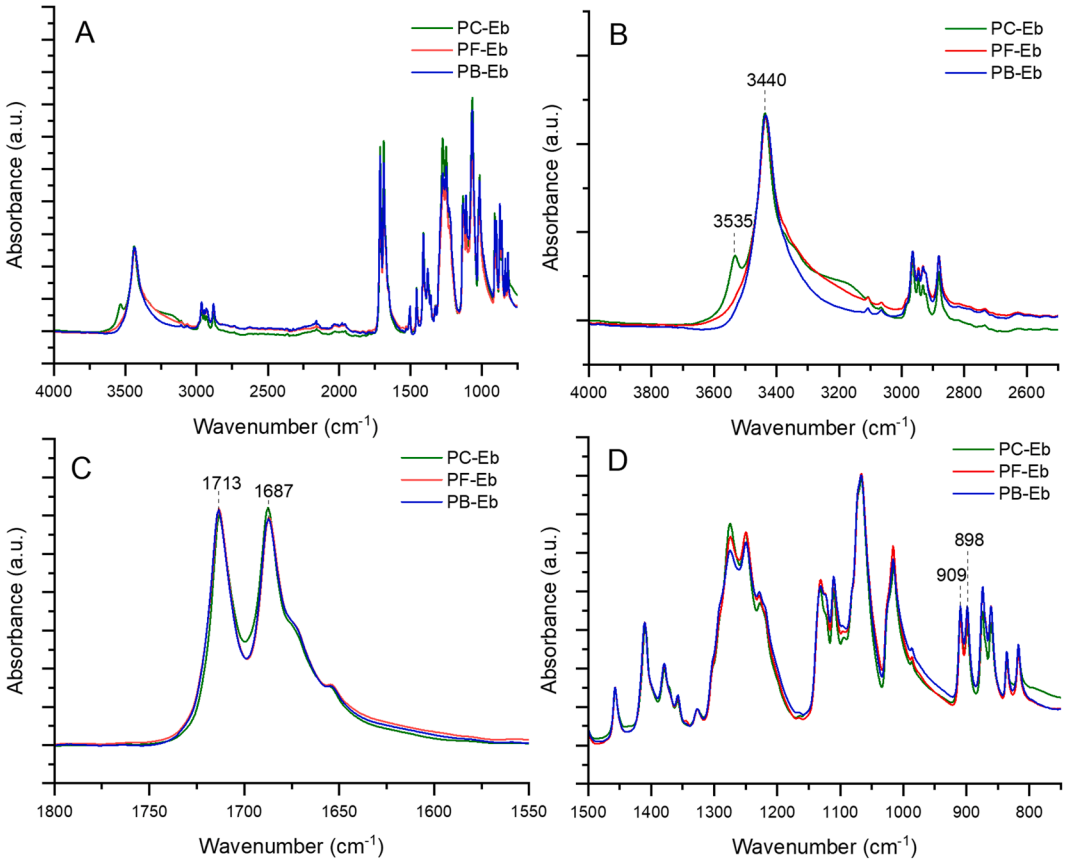

Fig. 5. Mean FTIR absorption spectra of PC, PB, PF collected after the second filtration step (fraction Eb) are shown in the full measured range (A), hydroxyl (B), carbonyl (C), and fingerprint (D) regions. In each spectral range, spectra have been normalized to maximum intensity. The relevant peaks are indicated.

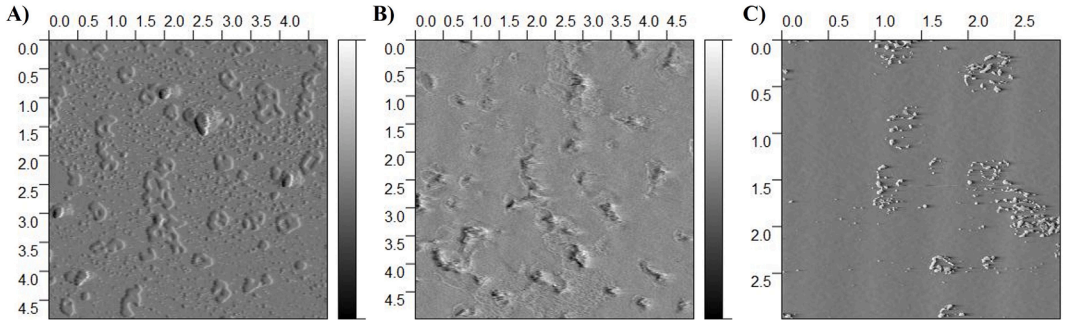

Fig. 6. Height-channel AFM maps of PC-Ea (A), PB-Ea (B) and PF-Ea (C). Scan areas are mentioned in μm on the panels. The greyscale wedge denotes the full topographic range (0–60 nm). Images were plane-levelled and rendered in Gwyddion 2.63.

by their thin morphology and larger accessible reactive surface area [45].

Overall, the combined FTIR and AFM data strongly supported the hypothesis that original PET material crystallinity and morphology significantly influence the final nanoparticle structure and chemical integrity post-EGF in both fractions Ea and Eb constituted, respectively, by the covalent polymer and by non-covalent monomers and oligomers aggregates. These insights not only affirm the critical impact of original polymer forms on the properties of generated MNPs but also underscore the importance of thorough characterization for developing standardized nanoparticle forms suitable for environmental and biological interaction studies.

3.5. Biological activity of PET MNPs: effect of MNPs treatment on THP-1 human macrophages

To study toxicological and proinflammatory properties of generated PET MNP, THP-1-derived human macrophages were used as an *in vitro* biosensor cell model. The experimental design was based on two read-outs: effect of MNP on THP-1 macrophage viability and induction of pyroptosis to measure toxicity and M1 THP-1 macrophage polarization. Initially MTT results showed that all PET MNP samples reduced THP-1 macrophage viability in a dose-dependent manner (Fig. 7). While low PET MNP concentrations (below 0.5 mg/ml) did not have a significant impact on macrophage viability, higher PET MNP concentrations (0.5–5 mg/ml) negatively affected cell viability. Importantly, fraction Eb (1–5 mg/ml) reduced cell viability more effectively compared to fraction Ea . This could be linked to differences in the composition of nanoparticles,

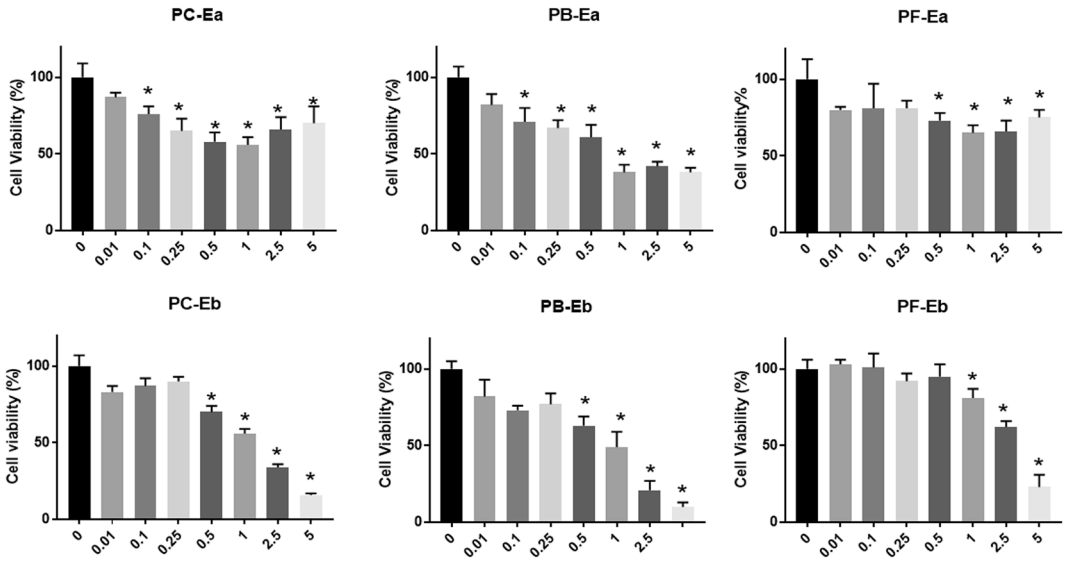

Fig. 7. PET MNP reduce THP-1 macrophages viability. THP-1 macrophages were treated with PET MNP with concentration ranging (0–5mg/ml) for 24 h as presented PC-Eb, PB-Eb, PF-Eb, PC-Ea, PB-Ea and PF-Ea respectively. Cell mediums were analysed by MTT assay. Results are from three independent treatments. Statistically significant results are indicated as $*p < 0.001$ versus control.\.

particle size between Ea (200–350 nm) and Eb (higher than 1000 nm) and also by the fact that Ea is formed by stable particles of covalent polymer while Eb is an unstable aggregate of non-covalent assembled monomers. Due to their colloidal instability, Eb aggregates may precipitate during incubation and accumulate on the cell surface, creating localized concentration hotspots that promote particle cell contact [46]. In contrast, the smaller, semi-crystalline Ea nanoparticles are more evenly dispersed and may interact with cells in a more uniform manner. This distinction underscores the relevance of aggregation behavior and physical form in determining the biological impact of PET-derived MNPs.

In a second series of experiments, we examined the ability of PET MNPs to induce LDH release as a biomarker of pyroptosis in THP-1 macrophages. Similarly to the MTT results, only high concentrations (1–5 mg/ml) of fraction Ea and Eb samples induced a significant release of LDH compared to the controls (Fig. 8). No significant differences were, however, observed between Ea and Eb fractions. These results demonstrated that PET MNP can induce LDH release in a dose-dependent manner irrespective of their physico-chemical properties and size which strongly influence their capacity to induce pyroptosis in THP-1 macrophages. Similar studies on nanoparticle aggregates showed the induction of oxidative stress and mitochondrial dysfunction without triggering acute necrosis or pyroptosis [46–48].

Our results are in support with recent study using PS MNP [49]. Adler *et al.* found that PS MNP induced LDH release in dose and size-dependent (500 nm as more effective compared to 1–3μm) manner in THP-1 macrophages. In contrast, the authors did not observe any effect of PS MNP on M1 macrophage polarisation using both THP-1 and PBMC-derived macrophages.

In the next series of experiments, we examined the potential of PET MNP to mediate the production of proinflammatory proteins (biomarkers of M1 polarisation) in THP-1 macrophages. For this purpose, we utilised an inflammation antibody array measuring the production of 40 proinflammatory proteins such as IL-1β, GM-CSF, IL-7, IL-8, MCP-1, MCP-2, MIP-1alfa, MIP-1beta and RANTES. Antibody array results revealed that both PET MNP Ea and Eb fractions induced the release of

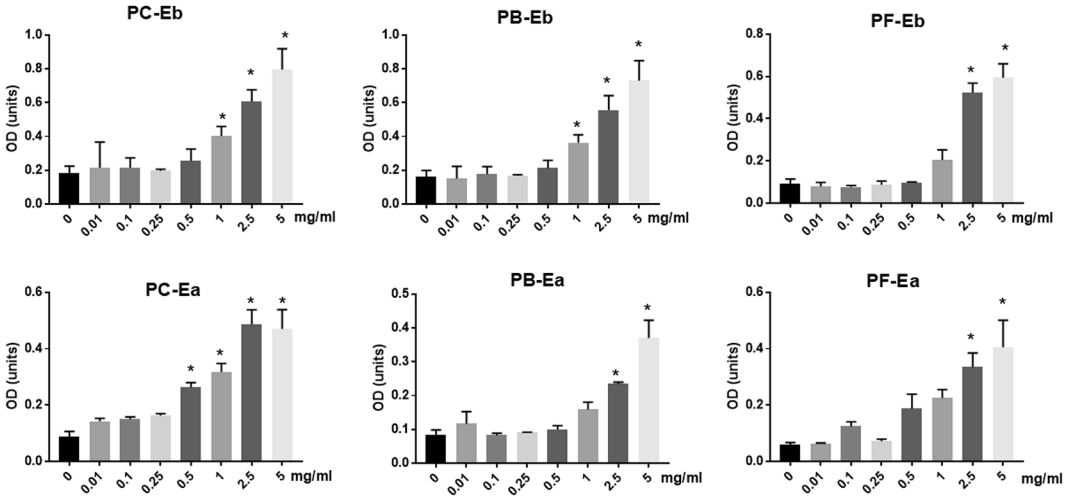

Fig. 8. PET MNPs induced LDH release in THP-1 macrophages. THP-1 macrophages were treated with PET MNP with concentration ranging (0–5mg/ml) for 24 h as presented PC-Eb, PB-Eb, PF-Eb, PC-Ea, PB-Ea and PF-Ea respectively. Cell mediums were analysed by LDH assay. Results are from three independent treatments. Statistically significant results are indicated as $*p < 0.001$ versus control.

10 out of 40 proinflammatory proteins all essential biomarkers for M1 macrophage polarisation and amplification of the immune response (Table 2). The amplitude of production of different proinflammatory mediators, however, varied between fractions Ea and Eb samples. These results demonstrated that PET MNPs induce proinflammatory mediators that are associated with M1 THP-1 macrophage polarisation.

We validated PET MNP-induced IL-1β production which is primarily linked to the induction of pyroptosis in THP-1 macrophages. Similarly to the LDH results, ELISA data showed that PET MNPs in both residues a and b samples upregulated IL-1β at 5mg/ml (Fig. 9). Interestingly, only PC-Ea and PB-Ea increased IL-1β release at 1mg/ml. These results clearly showed the potential of PET MNP a and b residues to induce THP-1 M1

Table 2
PET MNPs induce production of proinflammatory proteins in THP-1 macrophages. PET MNP (fractions Ea and Eb) upregulate release of proinflammatory mediators in THP-1 macrophages. THP-1 macrophages were treated with PET MNP (5mg/ml) for 24 h. Cell mediums were analysed on antibody inflammation array containing 40 proinflammatory proteins. Semi-quantitative results are normalized to untreated control cells (fold increase).

Proinflammatory protein	PC-Ea	PB-Ea	PF-Ea	PC-Eb	PB-Eb	PF-Eb	Proinflammatory protein	PC-Ea	PB-Ea	PF-Ea	PC-Eb	PB-Eb	PF-Eb
1. Eotaxin-1	0.96	0.87	1.04	0.96	0.74	0.83	**21. IL-13**	0.64	0.92	0.80	0.80	0.80	0.76
2. Eotaxin-2	0.96	1.11	0.81	0.89	0.93	0.85	**22. IL-15**	0.95	0.95	1.25	0.95	1.00	0.90
3. GCSF	0.83	0.65	0.91	0.65	0.74	0.87	**23. IL-16**	0.74	0.87	0.87	0.78	0.70	0.96
4. GM-CSF	**1.60**	**3.40**	1.35	1.40	**1.60**	1.05	**24. IL-17A**	0.69	0.96	0.85	0.69	0.85	0.62
5. ICAM	1.00	0.95	1.10	0.95	0.95	1.10	**25. IP10**	0.95	1.10	0.90	0.76	0.90	0.81
6. IFN-gamma	1.09	0.96	0.96	0.91	1.04	1.09	**26. MCP-1**	0.63	**2.08**	**1.66**	**1.95**	**1.25**	**0.37**
7. I309	1.14	0.90	1.10	0.95	1.05	1.10	**27. MCP-2**	**1.88**	**2.08**	**1.69**	**1.58**	**1.69**	1.42
8. IL-1α	1.00	1.25	1.30	1.15	1.25	1.05	**28. M-CSF**	0.96	1.00	1.24	1.00	1.04	0.72
9. IL-1β	**1.29**	**5.81**	**1.95**	**6.10**	**5.14**	**1.29**	**29. MIG**	1.00	0.84	0.89	1.00	0.84	0.89
10. IL-2	0.71	0.79	0.79	0.68	0.71	0.71	**30. MIP-1α**	**3.96**	**12.54**	**5.96**	**8.75**	**9.96**	0.88
11. IL-3	1.00	0.95	0.95	1.05	0.95	0.85	**31. MIP-1β**	**1.91**	**3.28**	**2.72**	**2.50**	**2.54**	0.52
12. IL-4	0.86	0.77	1.05	0.73	0.86	0.91	**32. MIP-1δ**	1.00	1.02	1.00	1.01	1.03	1.01
13. IL-6	0.82	0.95	0.82	0.82	0.91	0.73	**33. RANTES**	**0.48**	**2.07**	0.92	**2.76**	**3.78**	0.58
14. IL-6 R	0.60	1.29	1.21	1.19	0.73	0.40	**34. TGF-β**	0.86	1.00	0.90	1.00	0.90	0.95
15. IL-7	1.32	**1.58**	1.32	1.16	**2.05**	0.79	**35. TNF-α**	0.96	1.00	1.00	1.00	1.00	0.83
16. IL-8	**1.74**	**1.87**	**1.84**	**1.77**	**1.76**	1.44	**36. TNF-β**	0.86	0.90	1.10	0.95	0.95	0.81
17. IL-10	1.05	1.23	1.23	1.27	1.05	0.86	**37. TNF RI**	0.72	0.83	0.90	0.97	0.69	0.76
18. IL-11	0.79	0.83	0.75	0.71	0.75	0.71	**38. TNF RII**	1.00	1.03	1.19	1.06	1.13	1.00
19. IL-11 p40	0.95	1.15	1.15	1.00	1.05	0.85	**39. PDGF-BB**	0.95	0.95	1.05	1.21	1.00	1.00
20. IL-11 p70	1.05	1.00	0.91	0.91	1.05	0.91	**40. TIMP-2**	**0.38**	**0.35**	0.53	**0.31**	**0.35**	**0.32**

>2 - increase relative to control
>1.3 - increase relative to control
<0.5 - decrease relative to control

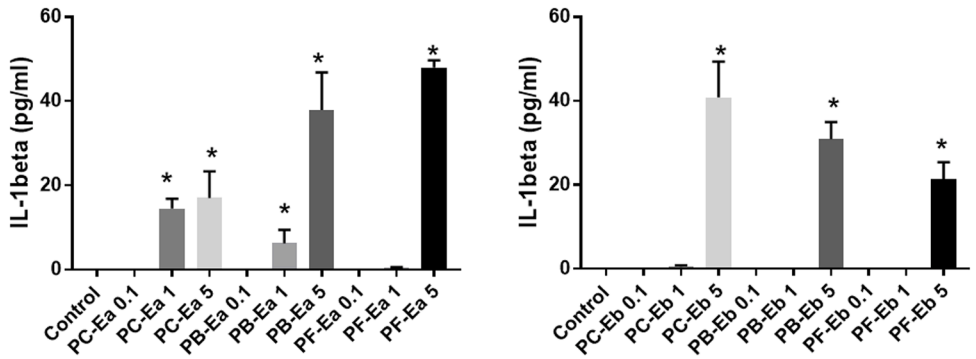

Fig. 9. PET MNP induce IL-1β release in THP-1 macrophages. THP-1 macrophages were treated with PET MNP with concentrations ranging (0–5mg/ml) for 24 h as presented PC-Eb, PB-Eb, PF-Eb, PC-Ea, PB-Ea and PF-Ea respectively. Cell mediums were analysed for IL-1β release by ELISA. The results are from three independent treatments. Statistically significant results are indicated as $*p < 0.001$ versus control.

polarisation associated with IL-1β and LDH release leading to induction of pyroptosis in THP-1 macrophages.

Although we validated only IL-1β release, further validation of other proinflammatory proteins could be useful to outline some differences between Ea and Eb fractions of PET MNP based on their different concentrations. For example, in a recent study Jeon *et al.* found that fragmented PP/PS MNP reduced cell viability in THP-1 monocytes that is associated with release of proinflammatory mediators (IL-1β and MIP-1β) [50]. Furthermore, using RAW264.7 mouse macrophages, Wu et al. demonstrated that variety of MNP (PP, PS, PE and PET) induced different modes of cell death dependent on their physico-chemical properties [51]. Similarly. Deng et al. provided evidence that MNP (PP, PS and PET) suppressed lysosomal activity associated with compromised cellular degradation processes in RAW264.7 mouse macrophages [52]. Our study demonstrates that both PET MNP fractions (Ea and Eb) reduce macrophage viability and induce LDH release as well as proinflammatory cytokines associated with M1 polarization and pyroptosis. This supports the use of the THP-1 macrophage polarization model as a robust biosensor for MNP immunotoxicity.

4. Conclusion

This study presents a reproducible and scalable method for generating PET MNPs via EGF, offering a significant route with higher yields than existing TFA hydrolysis approach. By employing sodium carbonate catalysis and ethylene glycol, we produced BHET-based oligomeric PET fragments from three distinct PET sources, commercial, bottle-grade, and film-grade. During the process, two filtration steps allowed to isolate two fractions Ea and Eb. Fraction Ea turned out to be composed of BHET-based PET fragments that effectively represent secondary PET nanoparticles generated by fragmentation processes (chemical, physical or mechanical). Fraction Eb consists of PET monomers re-associated through non-covalent interactions into large particles (1200–1900 nm size). This latter type of microplastic, generated by spontaneous monomer re-association, is reported and characterized here for the first time and could represent a secondary form of MNP found in the environment and in the human body.

The resulting MNPs (both fractions Ea and Eb) were comprehensively characterized and demonstrated significant physico-chemical differences attributable to their parent polymer form. Importantly, these structural variations correlated with differential biological responses in a THP-1 macrophage model, notably in cell viability, LDH release, and IL-1β production. This work emphasizes the need for source-specific MNP standards and highlights the value of physiologically relevant MNPs for toxicological studies. The use of a THP-1 macrophage polarization model as a biosensor also provides a powerful tool for immune toxicity assessment. By generating PET MNPs from defined packaging-grade sources under reproducible conditions, this study offers a framework for establishing physiochemically characterized MNP reference types relevant to specific environmental exposure scenarios. Altogether, our findings support the development of standardized, environmentally relevant PET NP reference materials for future ecotoxicological and biomedical research.

Funding information

No funding.

Support from ISIS@MACH ITALIA Research Infrastructure, the hub of ISIS Neutron and Muon Source (UK), [MUR official registry U. 0008,642.28–05–2020 – 16th April 2020].

CRediT authorship contribution statement

Mohammed Monsoor Shaik: Writing – review & editing, Writing – original draft, Visualization, Methodology, Investigation, Data curation, Conceptualization. **Diletta Ami:** Investigation, Data curation, Writing – review & editing, Writing – original draft, Methodology. **Alessio Romerio:** Writing – review & editing, Formal analysis, Data curation. **Calogero Gagliano:** Validation, Investigation, Data curation. **Charys Palmer:** Investigation. **Zaineh Aladailleh:** Investigation. **Elijah Mitchell:** Investigation. **Janet Lopez Chavez:** Investigation. **Asma Zain:** Investigation. **Stefano Farris:** Writing – review & editing, Methodology, Investigation. **Mattia Gaboardi:** Writing – review & editing, Software, Investigation, Formal analysis. **Antonino Natalello:** Writing – review & editing, Methodology, Data curation. **Grisha Pirianov:** Writing – review & editing, Writing – original draft, Methodology, Investigation, Data curation, Conceptualization. **Francesco Peri:** Writing – review & editing, Supervision, Project administration, Funding acquisition, Conceptualization.

Declaration of competing interest

The authors declare the following financial interests/personal relationships which may be considered as potential competing interests: Francesco Peri has patent METHOD FOR PRODUCING MICRO/NANOPLASTICS (MNPs) STANDARDS FROM POLYETHYLENE TEREPHTHALATE (PET) pending to University of Milano Bicocca. If there are other authors, they declare that they have no known competing financial interests or personal relationships that could have appeared to influence the work reported in this paper.

Acknowledgements

The authors gratefully acknowledge the support of the ISIS@MACH ITALIA Research Infrastructure, the hub of ISIS Neutron and Muon Source (UK), [MUR official registry U. 0008642.28–05–2020 – 16th

April 2020]. The authors would like to thank Dr. Barbara Vergani and Prof. Biagio Eugenio Leone for their help in the preparing and acquiring the TEM images.

Supplementary materials

Supplementary material associated with this article can be found, in the online version, at doi:10.1016/j.ceja.2026.101053.

Data availability

Data will be made available on request.

References

[1] M. Sewwandi, H. Wijesekara, A.U. Rajapaksha, S. Soysa, M. Vithanage, Microplastics and plastics-associated contaminants in food and beverages; Global trends, concentrations, and human exposure, Environ. Pollut. 317 (2023) 120747.

[2] N. Ali, J. Katsouli, E.L. Marczylo, T.W. Gant, S. Wright, J.B. De, La Serna, The potential impacts of micro-and-nano plastics on various organ systems in humans, EBioMedicine 99 (2024).

[3] P. Ahmadi, D. Doyle, N. Mojarad, S. Taherkhani, A. Janzadeh, M. Honardoost, M. Gholami, Effects of Micro-and nanoplastic exposure on macrophages: a review of molecular and cellular mechanisms, Toxicol. Mech. Methods (2025) 1–24.

[4] A. Amobonye, P. Bhagwat, S. Raveendran, S. Singh, S. Pillai, Environmental impacts of microplastics and nanoplastics: a current overview, Front Microbiol. 12 (2021) 768297.

[5] J. Zhao, R. Lan, H. Tan, J. Wang, Y. Ma, Q. Chen, F. Jiang, Z. Wang, B. Xing, Detection and characterization of microplastics and nanoplastics in biological samples, Nat. Rev. Bioeng. (2025) 1–15.

[6] Y.-H.V. Soong, M.J. Sobkowicz, D. Xie, Recent advances in biological recycling of polyethylene terephthalate (PET) plastic wastes, Bioengineering 9 (3) (2022) 98.

[7] E. MCARTHUR, The New Plastics Economy, Rethinking the Future of Plastics, 2014.

[8] G. Suzuki, N. Uchida, K. Tanaka, H. Matsukami, T. Kunisue, S. Takahashi, P. H. Viet, H. Kuramochi, M. Osako, Mechanical recycling of plastic waste as a point source of microplastic pollution, Environ. Pollut. 303 (2022) 119114.

[9] Y. Guo, X. Xia, J. Ruan, Y. Wang, J. Zhang, G.A. LeBlanc, L. An, Ignored microplastic sources from plastic bottle recycling, Sci. Total Environ. 838 (2022) 156038.

[10] K.N. Fotopoulou, H.K. Karapanagioti, Degradation of Various Plastics in the environment, Hazardous chemicals Associated With Plastics in the Marine Environment, Springer, 2017, pp. 71–92.

[11] J.P. Da Costa, P.S. Santos, A.C. Duarte, T. Rocha-Santos, (Nano) plastics in the environment–sources, fates and effects, Sci. Total Environ. 566 (2016) 15–26.

[12] B. Singh, N. Sharma, Mechanistic implications of plastic degradation, Polym. Degrad. Stab 93 (3) (2008) 561–584.

[13] P. Roudebush, Pet food additives, J. Am. Vet. Med. Assoc 203 (12) (1993) 1667–1670.

[14] S. Dattilo, C. Gugliuzzo, E.F. Mirabella, C. Puglisi, A.A. Scamporrino, D. C. Zampino, F. Samperi, Characterization of VOCs and additives in Italian PET bottles and studies on potential functional aldehydes scavengers, Eur. Food Res. Technol. 248 (5) (2022) 1407–1420.

[15] W.A. MacDonald, New advances in poly (ethylene terephthalate) polymerization and degradation, Polym Int 51 (10) (2002) 923–930.

[16] D. Carta, G. Cao, C. D'Angeli, Chemical recycling of poly (ethylene terephthalate) (PET) by hydrolysis and glycolysis, Environ. Sci. Pollut. Res. 10 (6) (2003) 390–394.

[17] S. Shirazimoghaddam, I. Amin, J.A. Faria Albanese, N.R. Shiju, Chemical recycling of used PET by glycolysis using niobia-based catalysts, ACS Eng. Au 3 (1) (2023) 37–44.

[18] M. Loganathan, M. Rajendraprasad, Recovery of Bis (2-hydroxyethyl) terephthalate and terephthalic acid from waste PET bottles for synthesis of cerium-based metal-organic frameworks: a study towards supercapacitor applications, React. Funct. Polym. 205 (2024) 106101.

[19] M. Loganathan, M. Rajendraprasad, B.M. Kiran, Sustainable recovery of monomers from PET and PC waste via Thermocatalytic depolymerization for synthesis of polycarbonates and co-polycarbonates, Eur Polym J. 221 (2024) 113516.

[20] A.G. Rodríguez-Hernández, J.A. Muñoz-Tabares, J.C. Aguilar-Guzmán, R. Vazquez-Duhalt, A novel and simple method for polyethylene terephthalate (PET) nanoparticle production, Environ. Sci.: Nano 6 (7) (2019) 2031–2036, https://doi.org/10.1039/c9en00365g.

[21] J. Domenech, A. Villacorta, J.F. Ferrer, R. Llorens-Chiralt, R. Marcos, A. Hernandez, J. Catalan, In vitro cell-transforming potential of secondary polyethylene terephthalate and polylactic acid nanoplastics, J. Hazard Mater. 469 (2024) 134030, https://doi.org/10.1016/j.jhazmat.2024.134030.

[22] A. Villacorta, L. Rubio, M. Alaraby, M. Lopez-Mesas, V. Fuentes-Cebrian, O. H. Moriones, R. Marcos, A. Hernandez, A new source of representative secondary PET nanoplastics. Obtention, characterization, and hazard evaluation, J. Hazard Mater. 439 (2022) 129593, https://doi.org/10.1016/j.jhazmat.2022.129593.

[23] M. Khoonkari, A.H. Haghighi, Y. Sefidbakht, K. Shekoohi, A. Ghaderian, Chemical Recycling of PET Wastes with Different Catalysts, Int. J. Polym. Sci. 2015 (2015) 1–11, https://doi.org/10.1155/2015/124524.

[24] D. Ami, P. Mereghetti, A. Foli, M. Tasaki, P. Milani, M. Nuvolone, G. Palladini, G. Merlini, F. Lavatelli, A. Natalello, ATR-FTIR spectroscopy supported by multivariate analysis for the characterization of adipose tissue aspirates from patients affected by systemic amyloidosis, Anal. Chem. 91 (4) (2019) 2894–2900.

[25] J. Zampolli, M. Mangiagalli, D. Vezzini, M. Lasagni, D. Ami, A. Natalello, F. Arrigoni, L. Bertini, M. Lotti, P. Di Gennaro, Oxidative degradation of polyethylene by two novel laccase-like multicopper oxidases from Rhodococcus opacus R7, Environ. Technol. Innov. 32 (2023) 103273, https://doi.org/10.1016/j.eti.2023.103273.

[26] D. Nečas, P. Klapetek, Gwyddion: an open-source software for SPM data analysis, Open Phys. 10 (1) (2012) 181–188, https://doi.org/10.2478/s11534-011-0096-2.

[27] Z. Fehér, J. Kiss, P. Kisszékelyi, J. Molnár, P. Huszthy, L. Kárpáti, J. Kupai, Optimisation of PET glycolysis by applying recyclable heterogeneous organocatalysts, Green Chem. 24 (21) (2022) 8447–8459, https://doi.org/10.1039/D2GC02860C.

[28] M. Babaei, M. Jalilian, K. Shahbaz, Chemical recycling of Polyethylene terephthalate: a mini-review, J. Environ. Chem. Eng. 12 (3) (2024) 112507.

[29] X. Zhou, X. Lu, Q. Wang, M. Zhu, Z. Li, Effective catalysis of poly(ethylene terephthalate) (PET) degradation by metallic acetate ionic liquids, Pure Appl. Chem. 84 (3) (2012) 789–801, https://doi.org/10.1351/PAC-CON-11-06-10.

[30] Z. Chen, J.N. Hay, M.J. Jenkins, FTIR spectroscopic analysis of poly(ethylene terephthalate) on crystallization, Eur. Polym. J. 48 (9) (2012) 1586–1610, https://doi.org/10.1016/j.eurpolymj.2012.06.006.

[31] C.A. Téllez S, E. Hollauer, M.A. Mondragon, V.M. Castaño, Fourier transform infrared and Raman spectra, vibrational assignment and ab initio calculations of terephthalic acid and related compounds, Spectrochim. Acta A: Mol. Biomol. Spectrosc. 57 (5) (2001) 993–1007, https://doi.org/10.1016/S1386-1425(00)00428-5.

[32] J. Welch, J. Wallace, A.B. Lansley, C. Roper, Evaluation of the toxicity of sodium dodecyl sulphate (SDS) in the MucilAir™ human airway model in vitro, Regul. Toxicol. Pharmacol. 125 (2021) 105022, https://doi.org/10.1016/j.yrtph.2021.105022.

[33] H. Sun, S. Zhou, Y. Jiang, Z. Qin, J. Fei, Y. Sun, J. Wang, X. Yin, Effect of cationic, anionic and non-ionic surfactants on transport of microplastics: role of adhesion of surfactants on the polyethylene surface, J. Hydrol. 612 (2022) 128051, https://doi.org/10.1016/j.jhydrol.2022.128051.

[34] A.P.R. Abud, J. Zych, T.L. Reus, C. Kuligovski, E. de Moraes, B. Dallagiovanna, A. M.d. Aguiar, The use of human adipose-derived stem cells based cytotoxicity assay for acute toxicity test, Regul. Toxicol. Pharmacol. 73 (3) (2015) 992–998, https://doi.org/10.1016/j.yrtph.2015.09.015.

[35] Y. Jiang, S. Zhou, J. Fei, Z. Qin, X. Yin, H. Sun, Y. Sun, Transport of different microplastics in porous media: effect of the adhesion of surfactants on microplastics, Water Res. 215 (2022) 118262, https://doi.org/10.1016/j.watres.2022.118262.

[36] L.M.A. Martin, N. Gan, E. Wang, M. Merrill, W. Xu, Materials, surfaces, and interfacial phenomena in nanoplastics toxicology research, Environ. Pollut. 292 (2022) 118442, https://doi.org/10.1016/j.envpol.2021.118442.

[37] A. Pradel, C. Catrouillet, J. Gigault, The environmental fate of nanoplastics: what we know and what we need to know about aggregation, NanoImpact 29 (2023) 100453, https://doi.org/10.1016/j.impact.2023.100453.

[38] T.L. Phillips, S. Hanna, Simulations of the mobile phase of polyethylene, Polym. (Guildf) 46 (24) (2005) 11035–11050, https://doi.org/10.1016/j.polymer.2005.09.019.

[39] G. Grause, J. Sutton, A.P. Dove, N.A. Mitchell, J. Wood, Crystallization of Bis(2-hydroxyethylene) Terephthalate as a Part of a Bottle-to-Bottle Recycling Concept for Poly(ethylene terephthalate), Cryst. Growth Des. 24 (17) (2024) 7306–7321, https://doi.org/10.1021/acs.cgd.4c00984.

[40] S. Monira, R. Roychand, F.I. Hai, M. Bhuiyan, B.K. Pramanik, Microplastic fragmentation into nanoplastics by water shear forces during wastewater treatment: mechanical insights and theoretical analysis, Environ. Pollut. 364 (2025) 125310, https://doi.org/10.1016/j.envpol.2024.125310.

[41] F. Dai, Q. Zhuang, G. Huang, H. Deng, X. Zhang, Infrared Spectrum Characteristics and Quantification of OH Groups in Coal, ACS Omega 8 (19) (2023) 17064–17076, https://doi.org/10.1021/acsomega.3c01336.

[42] M.P. Tsyurupa, Y.A. Borisov, Z.K. Blinnikova, N.P. Platonova, A.V. Ul'yanov, A. K. Buryak, V.A. Davankov, On the origin of absorbance band around 1700 cm−1 in FTIR spectra of hypercrosslinked polystyrene, Prot. Met. Phys. Chem. Surf. 50 (1) (2014) 59–63, https://doi.org/10.1134/S2070205114010225.

[43] I. Donelli, P. Taddei, P.F. Smet, D. Poelman, V.A. Nierstrasz, G. Freddi, Enzymatic surface modification and functionalization of PET: a water contact angle, FTIR, and fluorescence spectroscopy study, Biotechnol. Bioeng. 103 (5) (2009) 845–856, https://doi.org/10.1002/bit.22316.

[44] S. Ducoli, S. Federici, M. Cocca, G. Gentile, A. Zendrini, P. Bergese, L.E. Depero, Characterization of polyethylene terephthalate (PET) and polyamide (PA) true-to-life nanoplastics and their biological interactions, Environ. Pollut. 343 (2024) 123150, https://doi.org/10.1016/j.envpol.2023.123150.

[45] N.A. Tarazona, R. Wei, S. Brott, L. Pfaff, U.T. Bornscheuer, A. Lendlein, R. Machatschek, Rapid depolymerization of poly(ethylene terephthalate) thin films by a dual-enzyme system and its impact on material properties, Chem Catal. 2 (12) (2022) 3573–3589, https://doi.org/10.1016/j.checat.2022.11.004.

[46] A.E.T. van den Berg, K.J. Adriaans, L.A. Parker, E.M. Höppener, H.M. Dusza, J. Legler, R.H.H. Pieters, Top-down generated micro- and nanoplastics reduce

macrophage viability without eliciting a pro-inflammatory response, Microplastics Nanoplastics 5 (1) (2025) 32, https://doi.org/10.1186/s43591-025-00138-5.
[47] N.M. Schaeublin, L.K. Braydich-Stolle, A.M. Schrand, J.M. Miller, J. Hutchison, J. J. Schlager, S.M. Hussain, Surface charge of gold nanoparticles mediates mechanism of toxicity, Nanoscale 3 (2) (2011) 410–420, https://doi.org/10.1039/C0NR00478B.
[48] M. Kusaczuk, R. Krętowski, M. Naumowicz, A. Stypułkowska, M. Cechowska-Pasko, Silica nanoparticle-induced oxidative stress and mitochondrial damage is followed by activation of intrinsic apoptosis pathway in glioblastoma cells, Int. J. Nanomed. (2018) 2279–2294.
[49] M.Y. Adler, I. Issoual, M. Rückert, L. Deloch, C. Meier, T. Tschernig, C. Alexiou, F. Pfister, A.F.R.M. Ramsperger, C. Laforsch, U.S. Gaipl, K. Jüngert, F. Paulsen, Effect of micro- and nanoplastic particles on human macrophages, J. Hazard. Mater. 471 (2024) 134253, https://doi.org/10.1016/j.jhazmat.2024.134253.
[50] S. Jeon, D.-K. Lee, J. Jeong, S.I. Yang, J.-S. Kim, J. Kim, W.-S. Cho, The reactive oxygen species as pathogenic factors of fragmented microplastics to macrophages, Environ. Pollut. 281 (2021) 117006, https://doi.org/10.1016/j.envpol.2021.117006.
[51] Q. Wu, J. Cao, X. Liu, X. Zhu, C. Huang, X. Wang, Y. Song, Micro(nano)-plastics exposure induced programmed cell death and corresponding influence factors, Sci. Total Environ. 921 (2024) 171230, https://doi.org/10.1016/j.scitotenv.2024.171230.
[52] J. Deng, M.S. Ibrahim, L.Y. Tan, X.Y. Yeo, Y.A. Lee, S.J. Park, T. Wüstefeld, J.-W. Park, S. Jung, N.-J. Cho, Microplastics released from food containers can suppress lysosomal activity in mouse macrophages, J. Hazard. Mater. 435 (2022) 128980, https://doi.org/10.1016/j.jhazmat.2022.128980.